INTERNATIONAL ATOMIC ENERGY AGENCY
UNITED NATIONS EDUCATIONAL, SCIENTIFIC AND CULTURAL ORGANIZATION

INTERNATIONAL CENTRE FOR THEORETICAL PHYSICS
34100 TRIESTE (ITALY) - P.O.B. 586 - MIRAMARE - STRADA CONTIERA 11 - TELEPHONE: 2240-1
CABLE: CENTRATOM - TELEX 460392-1

SMR.300/50

College on Medical Physics
(10 October - 4 November 1988)

Strategies for Dose Surveys

C. MACCIA

CEPN, Fontenay aux Roses, France

** These notes are intended for internal distribution only

STRATEGIES FOR DOSE SURVEYS

*Carlo MACCIA
*CEPN - B. P. 48 - 92263 Fontenay aux Roses Cedex - France.

1. INTRODUCTION

The need to estimate patient doses in diagnostic radiology may take several diverse forms. At one extreme is the retrospective estimation of an individual foetal dose following abdominal examination. This involves a collation of all the known radiographic factors and number of films, and possibly an examination of each film for localisation purposes. At the other extreme is the large pre-planned assessment of doses to a large number of patients (involving different sites or organs), possibly involving several diverse examinations. It is clear that the stategy resources and techniques used will differ considerably between these two examples of dose examination. The purpose of this paper is to review the various strategies available and indicate their applicability and to summarize the experimental determinations of the basic x-ray interaction data namely : backscatter factors (BSF), tissue-air and scatter-air ratios (TAR and SAR).

2. Objectives of patient dosimetry

At least four primary objectives can be identified :

(i) To check the performance of new or modified equipment or techniques. Although some estimation of change is usually possible from physical considerations alone, a check of surface or organ dose using a realistic phantom may often be of value. It is important in this case to eliminate variations due to patient variability by using a reproductible phantom, as well as for the ethical reason of not subjecting patients to a new technique for test purposes.

(ii) To estimate "typical" doses for certain examinations. In this situation dose to individual patients are not required and again an anthropomorphic phantom may be used to derive typical organ doses, either by direct measurement in the phantom or from air dose measurements together with appropriate, pre-determined conversion factors.

(iii) To estimate doses for certain groups of patients. In this case a comparison may be required between groups of patients undergoing a particular examination at different hospitals. Patient variability (leading to intra-hospital variations) may make analysis difficult, but measurements on patients are necessary in order to reproduce the clinical conditions as accurately as possible. Direct measurement on patients are indicated.

(iv) To estimate a range of doses received for certain examinations. Here patient variations must be included in the measurements, which as in (iii) above should be of the direct kind.

3. Measurement Strategy

There are three types of measurement or estimation which may be made, involving anthropomorphic or mathematical phantoms, or patients.

3.1 Direct Measurement

Direct measurements involve a measurement of the dose at one or more points on the patient or phantom during the examination. In the case of patients they are often limited to surface dose measurements. Direct organ dose measurement is usually limited to superfical organs such as the eye, breast, testes etc... Direct measurements thus frequently form the basis of deep organ dose calculations. One of the main advantages of a direct approach is that a minimum of additional information is required. Radiographic variations during the procedure are automatically taken into account. On the other hand, it is obvious that the method does not apply to retrospective estimates of dose, and considerable resources in terms of dosimeter provision and read-out procedures may be necessary, particularly in extensive dose surveys.

3.1.1 Thermoluminescence dosimetry (TLD)

This is almost always the method of choice for direct measurements. TLD chips or powder sachets are small and unobtrusive, and may easily be attached to the patients' skin. It is unlikely, in most radiograhic examinations, that they will be seen on the film. A comprehensive review of TLD techniques is given by Mc Kinlay (1981). The energy response of the two most common phosphors, manganese-doped lithium borate and magnesium or titanium doped lithium fluoride are shown in figure 1.

Lithium borate in particular is the most tissue-equivalent phosphor available (Z_{eff} = 7.3) and has an energy response which varies by < 5 % from ICRU muscle in the energy range 20 keV to 1 MeV. Fading can be reduced to < 5 % per month and the simple glow curve facilitates easy readout and annealing. The detection threshold is 100 μGy.

Lithium fluoride is less tissue equivalent than lithium borate (Z_{eff} = 8.2) and has a slightly less favourable energy response. A more complex glow curve structure necessitates a more complicated annealing programme, but fading

can be reduced to 5 % per year. It has the advantage that it is approximately twice as sensitive as lithium borate, with a detection threshold of 50 μGy.

3.1.2 Ionisation chambers.

Although ionisation chambers are standard items of equipement for in-beam measurements, they are inconvenient for direct measurements and would be imaged together with the surrounding anatomy. Their only real advantage is that an immediate reading is available, unlike TLD.

3.2 Indirect estimation of dose

If only limited TLD facilities are available, or if retrospective dose estimate are required, then indirect techniques must be employed. Figure 2 shows a radiation beam iradiating a semi-infinite phantom. If an air dose measurement is made at K, then, the central axis surface dose and depth dose may be calculated if PDD and BSF data are available and if the appropriate radiographic factors have been recorded. Alternatively, TAR data may be used as shown. If planning a survey based upon indirect methods, a thorough evaluation of all the tubes and generators to be used must be undertaken, to establish the tube output for a range of tube voltages and values of mAs. No measurements are made during the examination, but radiographic factors (kVp, mAs, field size, SSD) must be recorded. A major problem with indirect methods arises when examinations do not consist simply of individual and well defined projections, but included the use of automatic exposure control or screening, the latter implying varying field sizes and positions.

3.3 Mathematical (Monte Carlo) Methods

Monte Carlo methods have been used extensively to calculate organ doses in diagnostic radiology (Rosenstein 1976, Drexler et al, 1984, Jones and Wall, 1985, Maccia et al, 1988). A three dimensional mathematical phantom consisting of elliptic cylinders, ellipsoids, truncated ellipsoids and cones, arranged in such a way as to give an approximation to anatomical accuracy. In spite of the limitations necessarily inherent in such an approach, a wide variety of examinations can be simulated. The technique is particularly appropriate for organ dose estimation where the site of the organ obviates a direct measurement. Primary beam spectra must also be simulated and the "history" of approximately 10^6 photons determined. The results may be cast as TARs, so that a measurement of air dose can be used to derive an organ dose.

3.4 Physical phantoms

The purpose of a phantom is to simulate the way in which radiation interacts with a patient and to predict, as accurately as possible, the dose distributions which will occur in practice. Water is a good substitute for soft tissues, if the semi-infinite nature of a water tank is acceptable. If specific organ doses are required, however, an anthropomorphic phantom is needed. This should accurately model human anatomy and be tissue-equivalent over the diagnostic energy range. Commercial phantoms are available, but care should be taken to esure that those designed primarily for radiotherapy fulfil this condition. White et al. (1977) have described a technique based upon expoxy resins which, with appropriate fillers, can be used to simulate a wide range of tissues.

4. X-ray beam interaction data for diagnostic radiology.

4.1 Percentage depth dose data (PDD). (Definition and published data).

Figure 3 shows an X-ray beam irradiating a semi-infinite water phantom. SSD is the source surface distance, w the width of the X-ray beam at the surface and D_o and D_d the absorbed doses at depth zero and d respectively. Figure 4 gives the definition of PDD.

PDD data in the relevant quality range for diagnostic radiology (1-4 mm al HVL) are available for radiotherapy purposes (B. J. R. suppl. 18, 1983) but may not always be suitable for diagnostic use since, in general, they apply to shorther SSDs and smaller field sizes than are commonly encountered in diagnostic radiology. Also, primary beam filtration in superficial radiotherapy is often less than is desirable, ar allowable, in diagnosis. Seelentag and Klotz (1959) measured PDD data for 150 cm^2 fields at 35 cm SSD and Trout et al. (1952) used a Victoreen thimble chamber for in phantom measurements. The unsuitable characteristics of this chamber make this data rather inaccurate, however further work by Trout et al. (1962) updated and extended the previous work. PDD data was also measured by Harrison (1981) who compared his data with that of the aforementioned authors as well as that contained in B. J. R. supplement 11 (1972).

4.1.1 Choice of detector

The choice of detector can sometimes lead to problems. The basic difficulty is

to use a chamber which is small enough to induce negligeable perturbations whilst, at the same time being large enough to provide a measurable ionisation current at large depths, without incurring anode heating problems due to long exposure times. Figure 5 and 6 illustrate some of the problems associated with a chamber of finite size. Thermoluminescence dosimetry should also be considered, but a solid water or tissue-equivalent material is then obligatory.

4.1.2 Definition of beam quality.

The complete specification of beam quality requires a knowledge of the entire x-ray spectrum. In practice, and for convenience, one or two parameters are chosen to represent beam quality. It has become clear (Greening, 1963; Harrison 1981) that the frist HVL alone is inadequate. It is necessary to include, in addition, the peak tube voltage or the second HVL (or homogeneity coefficient). Figure 7 gives an example of the specification of beam quality.

4.1.3 Zero area depth dose data.

Since scattered radiation contributes to patient dose but does not provide any diagnostic information in the image, a knowledge of the scatter contribution may be useful. To do this, zero area PDD data (due to primary radiation alone) may be subtracted from the PDD data to give the scattered component. Zero area data were estimated in two ways by Harrison (1981) :

a) by narrow beam attenuation measurements followed by an inverse-square connection to convert from infinite to finite SSD.

b) by calculation using the theoretical spectral data of Birch and Narshall (1979). For each spectrum and at each depth, photon fluence was converted to kerma-in-tissue (Birch et al 1979) and summed over all energies to give the PDD.

4.1.4 Measurements and accuracy.

Figure 8 and 9 give the details of the apparatus used by Harrison (1981) and the precision of the measurements.

4.1.5 Results and discussion.

Tabulated data covering the range 1-4 mm AL HVL for tube voltages of 60-100 kVp are given by Harrison (1981). Figure 10 shows a plot of PDD versus first HVL at three depths (1, 6 and 10 cm), at each of which, four values of tube voltage have been used. The broken curve refers to data from B. J. R. Suppl. 11 (1972). The two main point arising from these graphs are :

(i) that with increasing depth, there is a dependence of PDD on tube voltage for a given first HVL. This confirms the need to specify both HVL and kVp when defining the quality of a beam.
(ii) that there is good agreement with the BJR data for low values of total filtration (i. e. towards the low HVL portions of the curves).
Figure 11 shows a plot of zero-area PDD versus first HVL for the same conditions, calculated theoretically. Similar trends can be seen. Figure 12 gives a comparison of theoretical and experimental zero-area PDD data, again showing reasonable agreement and a confirmation of the kVp-dependence. The data of BJR Suppl. 11 were converted to 60 cm SSD using the conventional formula :

$$PDD(d, f_2, S_0) = PDD(d, f_1, S_0 / F)\,(B(S_0/F) / B(S_0))\,F^2$$

where

$F = ((f_1+d) / f_1)\,(f_2 / (f_2 + d))$

d = depth

f_1, f_2 = known and new SSDs respectively

B = backscatter factor

S_0 = field size at surface

The comparison of these converted data are in good agreement with the experimental work and with theory at depths > 6 cm, but significant differences arise at smaller depths.

4.2 Backscatter Factor (BSF)

Dubuque et al. (1977), Stanton (1982) and Harrison (1982) measured BSF (defined in figure 3 and 4) experimentally under a variety of conditions. Dubuque used a lucite, rather than a water phantom to measure BSFs in the mammographic quality range and Stanton measured over a wide range of HVL using an extrapolation technique. Two measurement techniques were used by Harrison, ionisation chamber and TLD.

4.2.1 Experimental method.

4.2.1.1 Ionisation chamber measurements.

Figure 15 illustrates some of the problems of using an ionisation chamber to measure BSF. Aart from displacement effects which are similar to those discussed in section 2.2, it is necessary to take into account the presence of the perspex waterproof cap. Figure 14 gives the steps in the procedure. M_1 is

the ratio of the exposure in air (E_A), without a cap, at A in figure 13) to the exposure in air with a full cap (E_C). This is used to carrect measurements necessarily made with a cap to those which would have beeen made without one (A). Similar M_2 is the ratio of E_A to E_B which gives a correction for the presence of half a cap. This is used to form the quantity E_D, the "ideal" surface measurement from the actual measurement E_E, which includes, in effect, half a cap (the other half being immersed in, and therefore approximately equivalent to, water).

4.2.1.2 Results and discussion of ionisation chamber measurements.

Figure 13 shows the experimental BSFs compared with the data of BJR Suppl. 11 (1972). Once again the tube voltage dependence can be noted, emphasising again the inadequacy of HVL alone as a specifier of beam quality. Poor agreement with the BJR data is attributable (at least in part) to displacement errors arising from the use of a chamber of finite volume. Ionisation chamber measurements are thus likely to be inaccurate, although reasonably precise. One possible solution is to use a smaller flatter chamber, although the framework surrounding the chamber volume must ideally be water-equivalent. Another possible solution is to use TLD as follows.

4.2.1.3 TLD Measurements.

Thin plastic film was used to support manganese-doped lithium borate chips, which could then be brought into contact with the surface of the phantom as shown in Figure 16. Lithium borate was chosen for its flat energy response (figure 1).

4.2.1.4 Results and discussion of TLD Measurements.

Figure 17 shows BSF plotted against first HVL, with data of BJR Suppl. 11 (1972), Dubuque et al. (1977) and Stanton et al. (1982) shown for comparison. The small size of the TLD chips (3.2 x 3.2 x 0.9 mm) minimizes displacement effects. However, even when each chip is calibated individually, measurement precision is inferior to ionisation chamber techniques. Thus the BSF are accurate but relatively imprecise, in contrast to those derived from ionisation chamber techniques. The data have been tabulated for a number of field sizes by Harrison (1982).

4.3 Tissue-air (TAR) and scatter air ratios (SAR).

PDD and BSF data allow estimates of dose at depth to be made from a

knowledge of the tube output in air.
Alternatively, the data may be recast into the form of TARs, whose definition is given in figure 18, and using the expression :

$TAR\ (d, S_d) = 1/100\ PDD\ (d, f, (S_d\ f/f+d))\ BSF\ (S_d\ f/f+d)\ ((f+d)/f)^2$.
$SAR\ (d, S_d) = TAR\ (d, S_d) - TAR\ (d,o)$

Figure 19 to 21 show the result of this computation (Harrison 1983a) with the data of Shultz an Gignac (1976) and Sabel et al. (1980) for compaison.

4.4 Energy Imparted.
Energy imparted is useful quantity in risk estimation, since it is closely related to the whole body effective dose equivalent, if it is assumed that radiosensitive tissues are homogeneously mixed.
Figure 22 demonstrates the routes by which energy imparted may be calculated. One approach is to measure the incident energy fluence (by means of an area-exposure meter device) and then allow for the escape of some of this energy (by trasmitted primary beam and seconadry radiation) by Monte Carlo calculations involving realistic body shapes and incident spectra. (Shrimpton et al (1984), Carlsson et al (1984). Another, more empirical approach is to integrate PDD data over all depts for a certain field size sothat the PDD integral is reduced by the ammount of energy escaping. Clearly, this latter technique does not allow for differences in patiet shape. However for practical purposes, the errors incurred may not be too serious.
Figure 22-24 outline the calculation of energy imparted; because of beam hardening effects, the PDD data should be expressed as a sum of two or three exponential components and the expression given in figure 24 (Harrison 1983b) used.
Figure 25 shows energy imparted per unit surface area and per unit surface dose as a function of first HVL. The broken lines refer to Monte Carlo calculations and energy fluence derivations by Shrimpton and Wall (1983) whilst the solid line represents Harrison's PDD interation (using 30 x 30 cm field).
Harrison's data is between 6 and 18% higher. Clearly insufficient allowance has been made for escape of secondary radiation; a smaller, although no less arbitrary, choice of field size (say 15 x 15 cm) would give closer agreement between the two quite different methods. Shrimton et al. (1984) have derived values of energy fluence per unit exposure for various beam qualities (figure 26) and factors for converting Diamentor measurements of exposure

area-product into estimates of energy imparted for a range of qualities (figure 27). Again, two parameters are needed to specify beam quality; in these cases peak tube voltage and total filtration have been chosen.

5. Summary of strategies.
Figure 28 summarizes the possible routes by which skin or organ doses may be estimated. Four examples will illustrate the possibilities.

5.1 Route a-e-j
This is a direct measurement on the patient surface, and could represent a superficial organ dose (eg thyroïd, breast) directly. It allows for patient variability and requires minimal recording of radiographic parameters. It could be employed in surveys of groups of patients and/or ranges of doses for certain examinations, and may be followed by a calculation of "deep" organ doses using PDD data.

5.2 Routes a-d-i or a-d-l
This represents a direct measurement on a phantom and would be employed if patient variability were to be excluded in oder to examine the effect of a change in general technique.

5.3 Routes b-g-j or b-g-m
This could represent a retrospective dose estimate (eg. foetal exposure) or dose estimates for simple examinations, particularly if TLD facilities were unavailable. Radiographic parameters need to be recorded.

5.4 Route c-h-n
This mathematical simulation could be used to calculate energy imparted, to make estimates of doses to many organs or tissues, or to study the effects of changes in primary beam spectra without performing extensive physical measurements.

References

McKinley AF. 1981 "Thermoluminescence Dosimetry" Medical Physics Handbook 5. Adam Hilger.

Rosenstein M. 1976 "Organ doses in diagnostic radiology" US Dept. of Health, Education and Welfare. BRH, HEW publication (FDA) 76-8030.

Drexler G., Panzer W, Widermann L., Williams G. and Zankl M. 1984 "The calculation of dose from external photon exposures using reference human phantoms and Monte Carlo methods. Part III: Organ doses in x-ray diagnosis. GSF-Bericht S1026 (Gesellschaft für Strahlen und Umweldforschung, München).

White DR., Martin RJ. and Darlison R. 1977 Brit. J. Radiol. 50, 814-821.

Shrimpton PC., Wall BF., Jones D.G., Fisher ES., Hillier MC. and Kendall GM. and Harrison RM. 1986 "A National Survey of Doses to Patients Undergoing a Selection of Routine X-ray Examinations in English Hospitals" NRPB-R200 Chilton, Didcot, Oxon OX11 ORD.

Maccia, C., Benedittini, M., Le Faure, C. & Fagnani. F. 1988. Doses to patients from diagnostic radiology in France. Health Physics, 4, 397-408.

Harrison RM., Clayton CB., Day MJ., Owen JP and York MF. 1983, Brit. J. Radiol. 56, 383-395.

Birch R. and Marshall M. 1979. Phys. Med. Biol 24 505-17

Birch R., Marshall M. and Ardran GM 1979 Catalogue of Spectral Data for Diagnostic X-rays SR5 30 (HPA, 47, Belgrave Square, London SW1X 8QX).

Burns JE in "Central Axis Depth Dose Data for use in Radiotherapy" B. J. Radiol Suppl 11 1972

Harrison RM 1981 Phys. Med Biol 26 : 657-670.

Seelentag W. and Klotz E. 1959 Strahlentherapie 108 : 112-26

Trout ED, Kelly JP and Cathey GA 1952 Am. J. Roentgenol. 67: 946-63

Greening JR 1963 Br. J. radiol 36 363-71

Trout ED, Kelly JP and Lucas 1962 in "Technological Needs for reduction of Patient Dosage from Diagnostic Radiology" (Springfied IL: CC Thomas).

BJR 1983 Central Axis Depth Dose Data for use in Radiotherapy Br. J. Radiol Supplement 18

Dubuque GL, Cacak RK. and Hendee W.R 1977 Med Phys. 4 : 397-399.

Stanton L, Bratelli S. D, Day J. L, Stanton R. E and Villafana T.1982 Med Phys 9 : 121-130

Harrison RM 1982 Phys. Med. Biol 27: 1465-1474

Schulz RJ and Gignac C. 1976. Radiology 120 : 687-90

Sabel M, Bednar W and Weishaar J 1980. Strahlentherapie 156: 502-508

Shrimpton PC and Wall BF 1983 Phys Med Biol 28: 1159-1162

Carlsson GA, Carlsson CA and Persliden J 1984 29:1329-1341

Harrison RM 1983 (a) Phys. Med Biol 28 1-18

Harrison RM 1983 (b) Phys Med Biol 28: 701-707

Shrimpton PC, Wall BF, Jones DG and Fisher ES 1984 Phys Med Biol 29 : 1199-1208

Mayneord W.V 1940 Br. J Radiol 13 : 235-247.

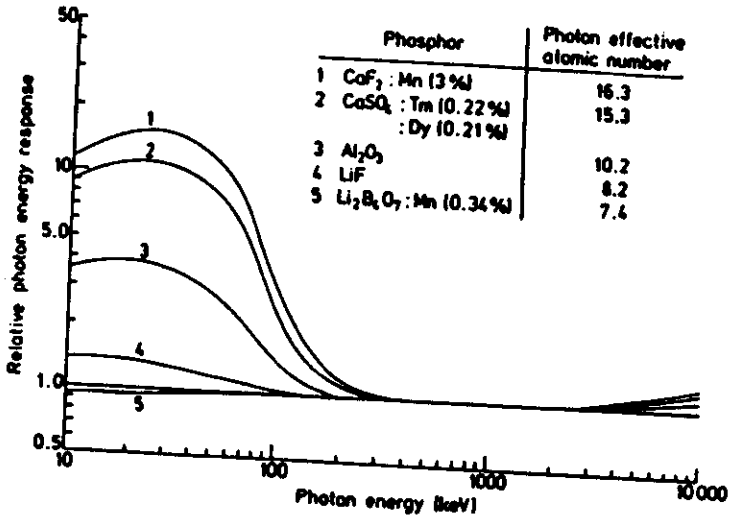

	Phosphor	Photon effective atomic number
1	CaF_2 : Mn (3 %)	16.3
2	$CaSO_4$: Tm (0.22 %) : Dy (0.21 %)	15.3
3	Al_2O_3	10.2
4	LiF	8.2
5	$Li_2B_4O_7$: Mn (0.34 %)	7.4

Figure 1 : Energy response of TLD phosphors.

INDIRECT MEASUREMENT

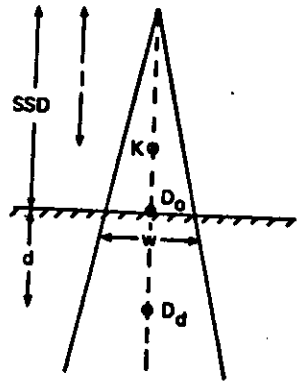

D_o = K(kVp, HVL, mAs) . $(\frac{1}{SSD})^2$. BSF (HVL, w) . f . mAs

f = air kerma to tissue dose conversion factor

D_d = D_o . PDD (kVp, HVL, d, w, SSD)/100

USING TARs

$D_d = K\ (kV_p, HVL, mAs) . (\frac{1}{SSD+d})^2 . TAR(kV_p, HVL, d, w') . f . mAs$

$w' = (\frac{SSD+d}{SSD})\ w$

Figure 2.

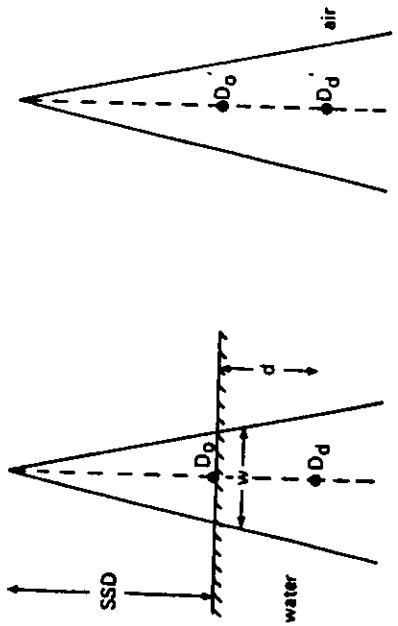

Figure 3 : Irradiation Geometry and Definitions.

Central axis % depth dose (PDD)

$$PDD\ (d, w, SSD, kVp, HVL) = \frac{D_d\ (d, w, SSD, kVp, HVL)}{D_o\ (w, SSD, kVp, HVL)}$$

Backscatter factor (BSF)

$$BSF\ (w, SSD, kVp, HVL) = \frac{D_o\ (w, SSD, kVp, HVL)}{D_o'\ (SSD, kVp, HVL)}$$

Figure 4.

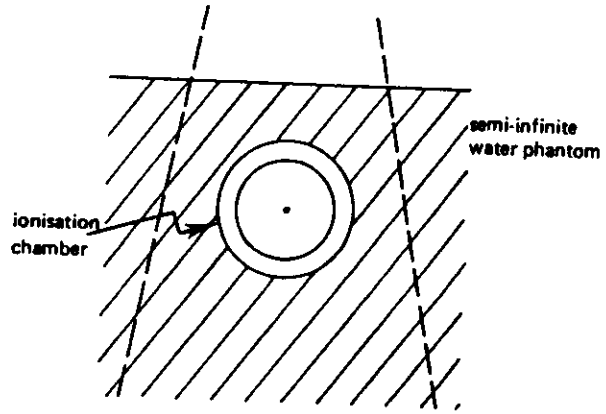

Figure 5 : An ionisation chamber immersed in a semi-infinite water phantom.

CHOICE OF DETECTOR (IONISATION CHAMBER)

1. Must be large enough to generate measurable ionisation current
2. Must be small enough to minimise errors due to displacement of water
   - (i) reduced attenuation due to air cavity
   - (ii) reduced scatter contribution from within chamber
   - (iii) reduced attenuation of scatter
   - (iv) increased scatter component from regions in the "shadow of the chamber"
   - (v) exposure gradient (3% mm^{-1} at 60 kVp)

Figure 6.

SPECIFICATION OF BEAM QUALITY

1st HVL
2nd HVL } homogeneity coefficient (HVL_1/HVL_2)

peak tube voltage

1st HVL = 2 mm Al < 100 kVp; 1.1 mm Al total filtration
                   < 50 kVp; 2.8 mm Al total filtration

Figure 7.

APPARATUS

Medio DLX; FWR waveform
Machlett Dynamax X-ray tube (2 mm focus)

Detector volume = 0.3 cm^3 (NE 2502)
Chamber thickness = 0.15 cm

Ionex dosemeter (2500/3)

Figure 8.

PRECISION

In a single measurement:

Depth (cm)	Precision
0–5	± 1%
5–10	± 3%
10–14	< ± 6%

Figure 9.

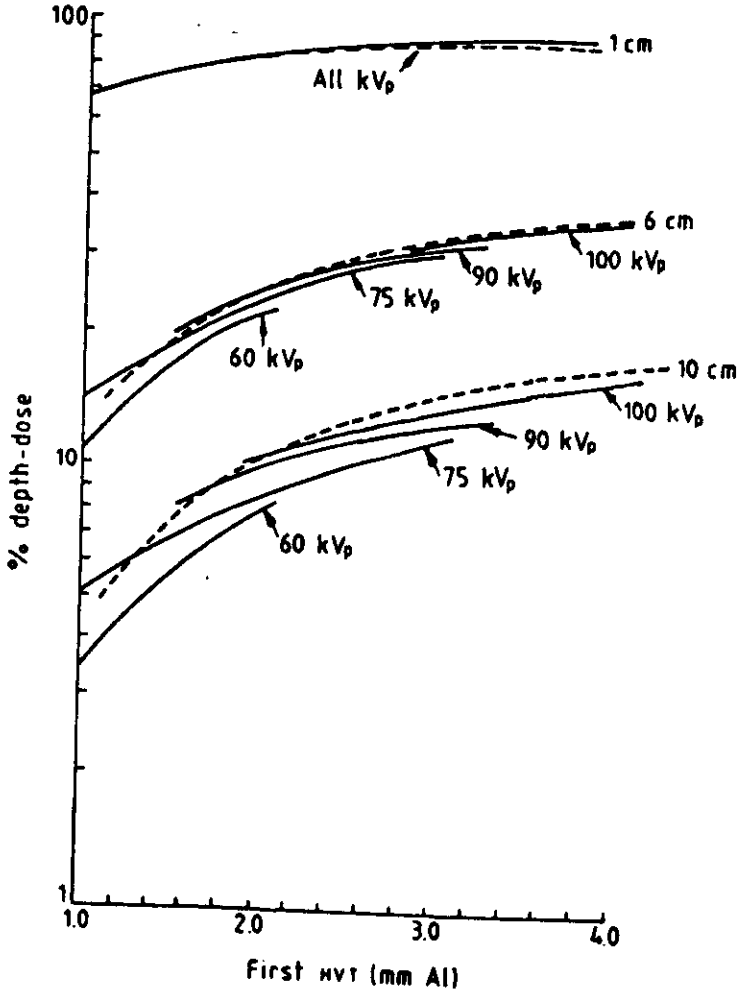

Figure 10 : PDD vs HVL for a 10 x 10 cm Field at 60 cm SSD Experimental data (full curves) B. J. R. Suppl. 11 (broken curves).

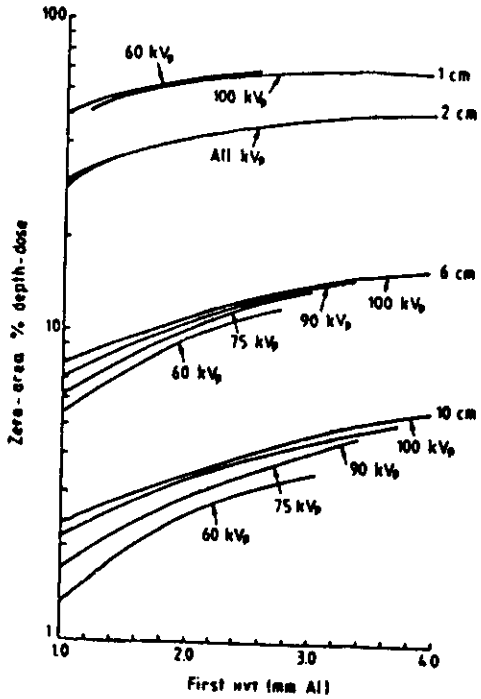

From theoretical spectra

Figure 11 : Zero Area PDD Vs HVL.

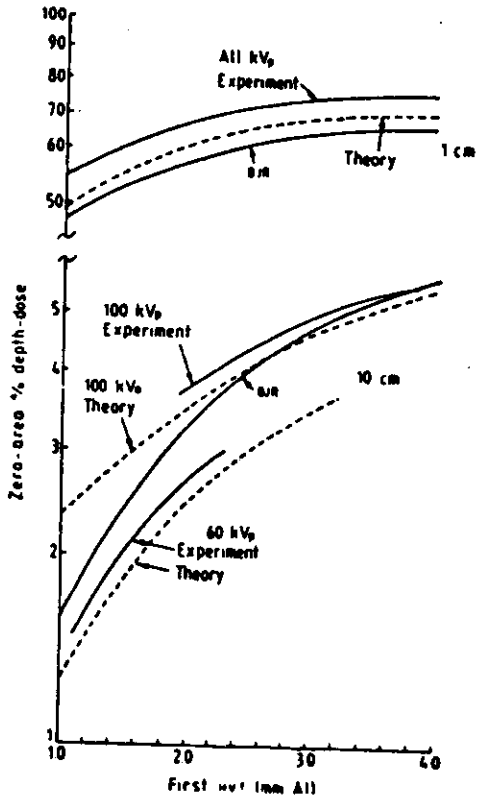

Figure 12 : Zero-Area PDD vs HVL, Comparison of thepry and experiment.

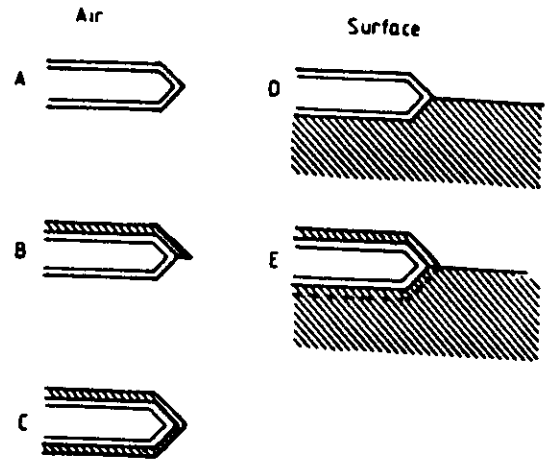

Figure 13 : Measurement of BSF using an ionisation chamber.

$$M_1 = E_A/E_C$$

$$M_2 = E_A/E_B$$

$$E_D = E_E M_2$$

$$E_A = E_C M_1$$

$$BSF = \frac{E_D}{E_A}$$

$$= \frac{E_E}{E_C}\left(\frac{M_2}{M_1}\right)$$

Figure 14 .

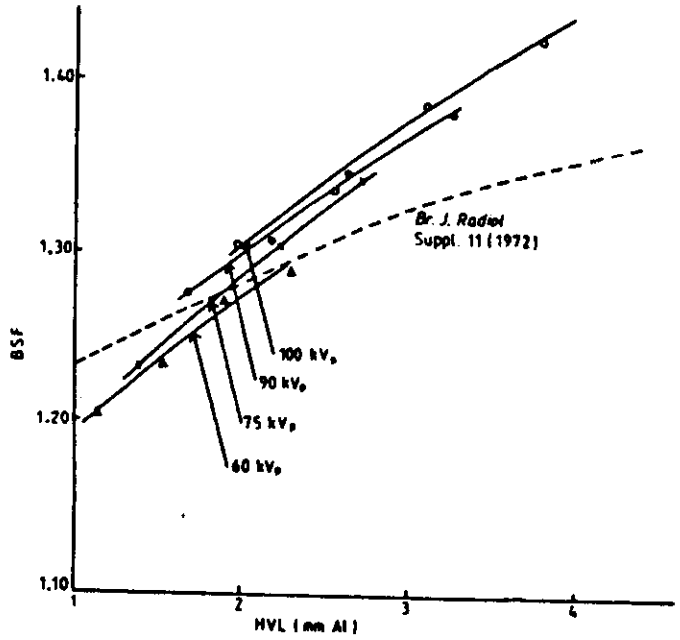

BSF v HVL Ionisation chamber measurements
15 x 15 cm field

Figure 15.

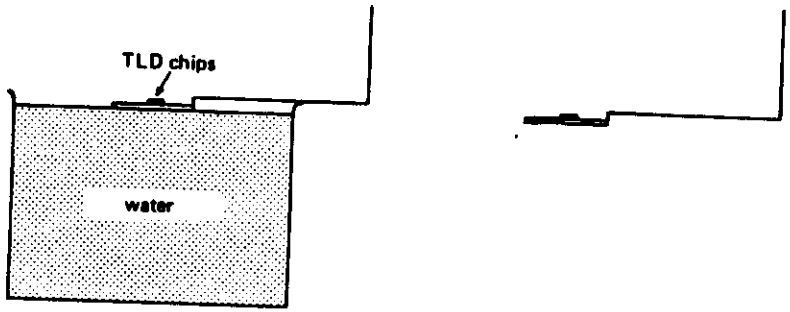

Figure 16 : Measurement of BSF using TLD.

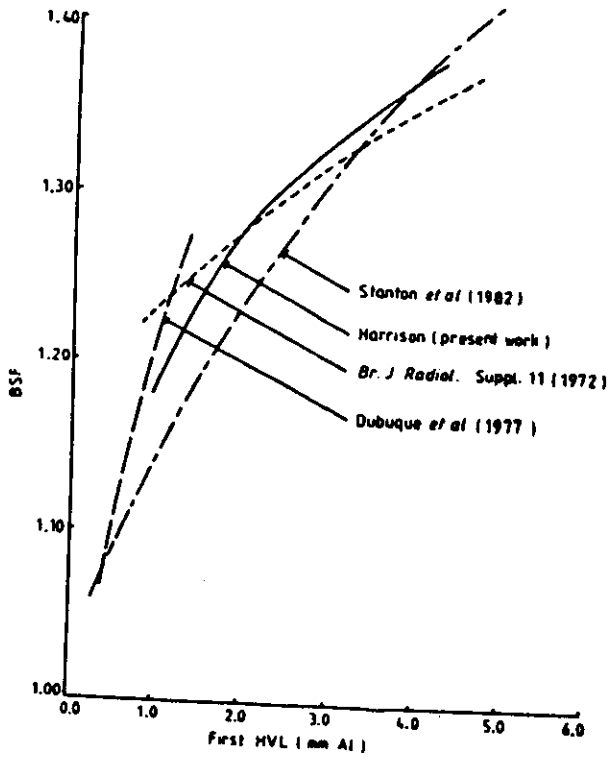

BSF v HVL TLD measurements
15 x 15 cm field

Figure 17.

Tissue air ratio (TAR)

$$TAR(w, SSD, d, kVp, HVL) = \frac{D_d(d, w, SSD, kVp, HVL)}{D_d'(d, SSD, kVp, HVL)}$$

Scatter air ratio (SAR)

$$SAR(d, w, SSD, kVp, HVL) = TAR(d, w, SSD, kVp, HVL) - TAR(d, w=0, SSD, kVp, HVL)$$

Figure 18

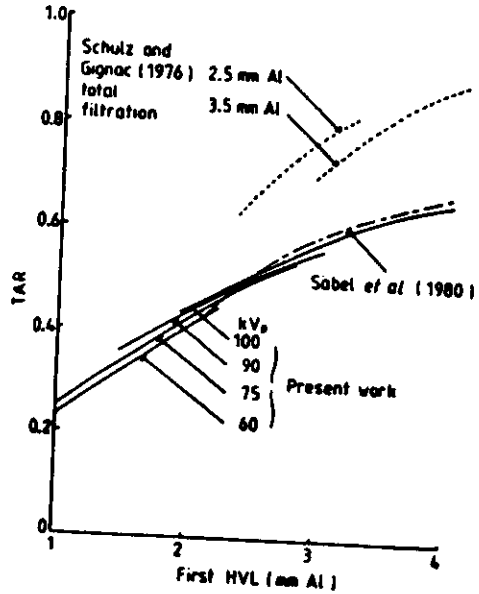

TAR v HVL 10 x 10 cm field
at 5 cm depth

Figure 19.

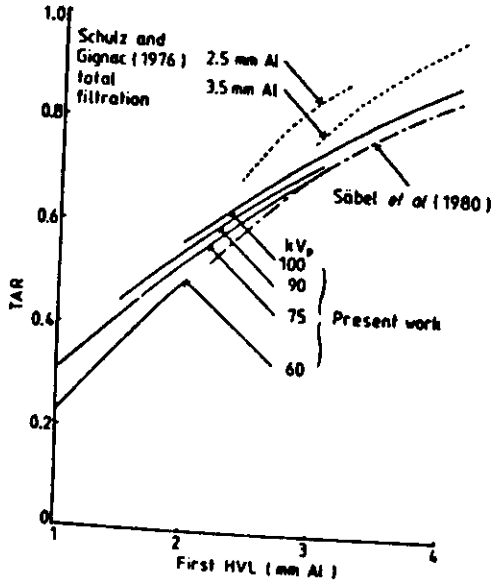

TAR v HVL 20 x 20 cm field at 5 cm depth

Figure 20.

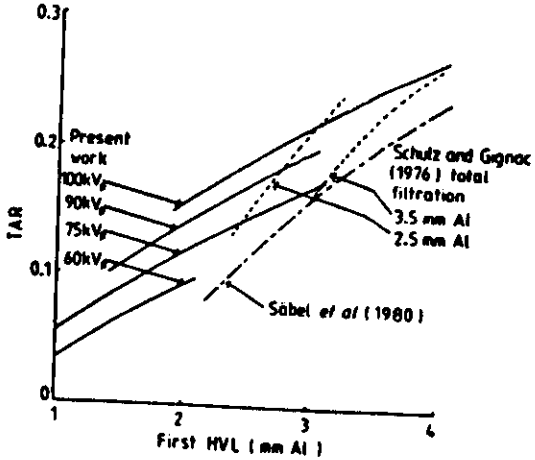

TAR v HVL 30 x 30 cm field at 14 cm depth

Figure 21.

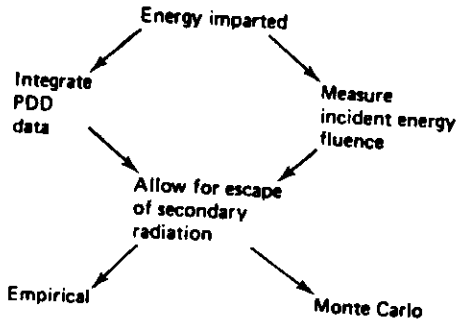

Figure 22 : Estimate of energy imparted.

INTEGRATION OF POD DATA

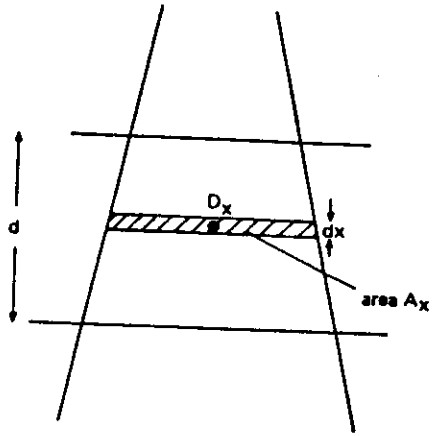

Total energy $\epsilon = \rho \int_0^d D_x A_x \, dx$

$D_x = D_0 \exp\{-\mu_e x\}$

$A_x = A_0 [(SSD + x)/SSD]^2$

$\epsilon \approx \frac{D_0 A_0}{\mu_e} \left(1 + \frac{2}{\mu_e}\right)$

Improve by considering multiexponential attenuation

$$\epsilon = D_0 A_0 \left[\sum_{j=1}^{n} k_j \int_0^d \left(\frac{SSD + x}{SSD}\right)^2 \exp\{-\mu_j x\} \, dx\right]$$

Figure 23.

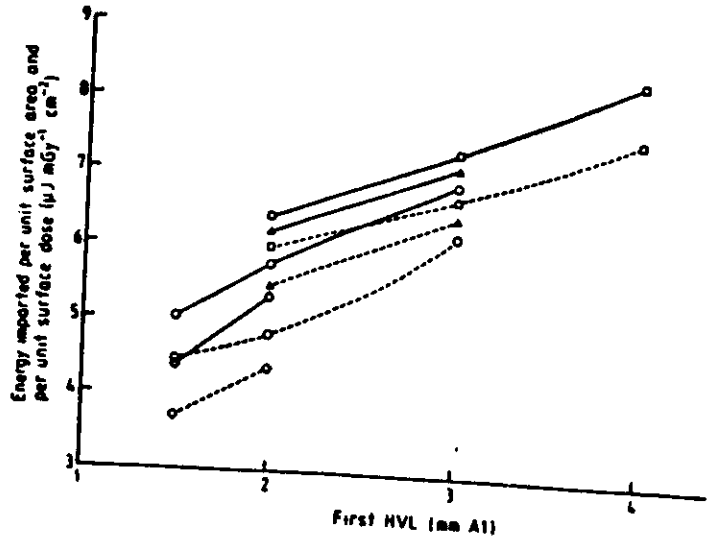

Shrimpton and Wall (1983)

Comparison of energy imparted factors due to Shrimpton (- - -) and Harrison (——) for several X-ray generating voltages: ◇, 60 kV_p; ○, 75 kV_p; △, 90 kV_p; and □, 100 kV_p.

Figure 24.

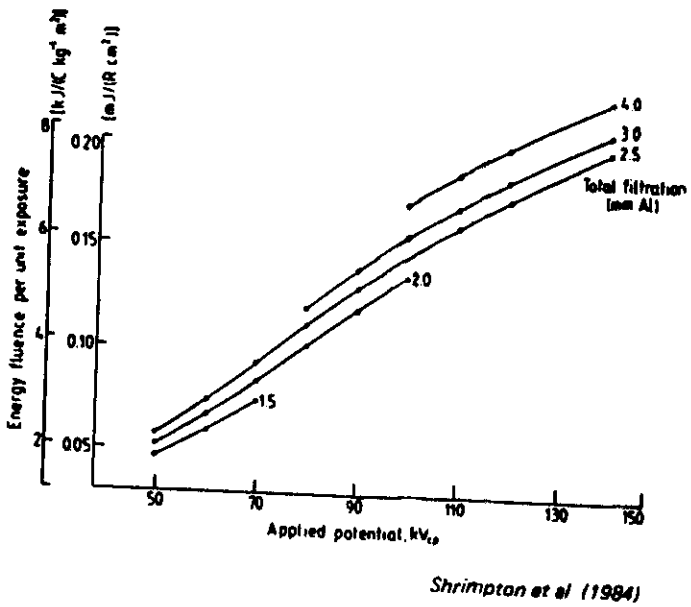

Figure 25 : Energy fluence per unit exposure vs kVp.

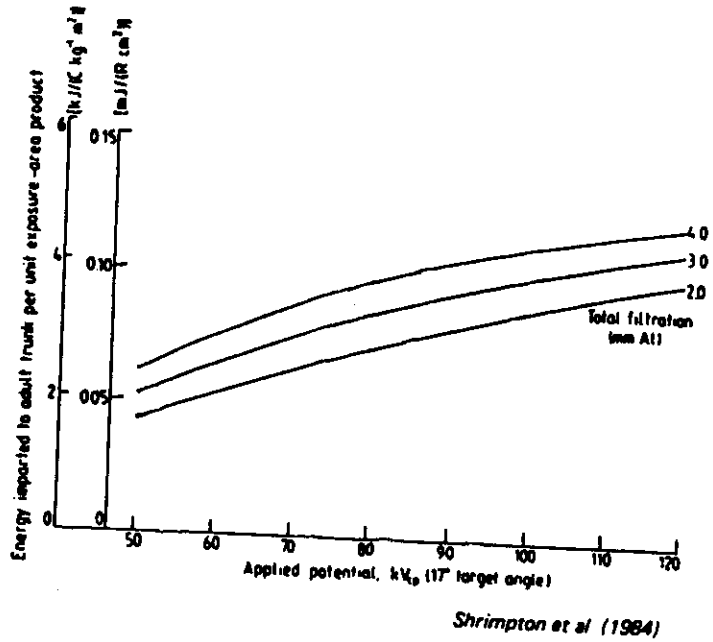

Figure 26 : Energy imparted to adult trunk per unit area-exposure product vs kVp.

STRATEGIES FOR SKIN AND ORGAN DOSE MEASUREMENTS

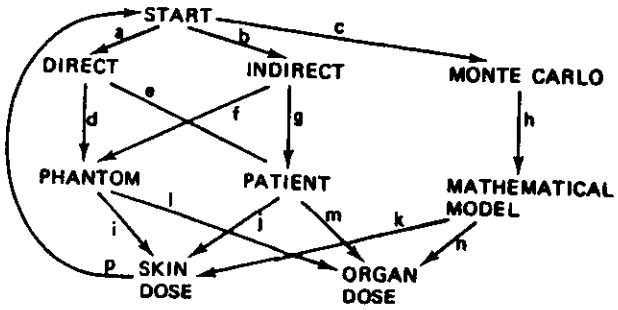

Figure 27.